

## Assimilation of drifter observations in primitive equation models of midlatitude ocean circulation

Tamay M. Özgökmen, Anne Molcard,<sup>1</sup> and Toshio M. Chin<sup>2</sup>

Meteorology and Physical Oceanography, Rosenstiel School of Marine and Atmospheric Sciences, University of Miami, Miami, Florida, USA

Leonid I. Piterbarg

Center for Applied Mathematical Sciences, University of Southern California, Los Angeles, California, USA

Annalisa Griffa<sup>1</sup>

Meteorology and Physical Oceanography, Rosenstiel School of Marine and Atmospheric Sciences, University of Miami, Miami, Florida, USA

Received 19 November 2002; revised 8 April 2003; accepted 23 April 2003; published 25 July 2003.

[1] Motivated by increases in the realism of OGCMs and the number of drifting buoys in the ocean observing system, a new Lagrangian assimilation technique is implemented in an idealized, reduced-gravity configuration of the layered primitive equation model MICOM. Using an extensive set of twin experiments, the effectiveness of the Lagrangian observation operator and of a dynamical balancing technique for corrected model variables, which is based on geostrophy and mass conservation, are explored in comparison to a conventional Pseudo-Lagrangian observation operator and an implementation of the Kalman filter method. The results clearly illustrate that the Lagrangian observation operator is superior to the Pseudo-Lagrangian in the parameter range that is relevant for typical oceanic drifter observations, and that the simple dynamical balancing technique works well for midlatitude ocean circulation. *INDEX*

*TERMS:* 4263 Oceanography: General: Ocean prediction; 4255 Oceanography: General: Numerical modeling; 4594 Oceanography: Physical: Instruments and techniques; 4572 Oceanography: Physical: Upper ocean processes; *KEYWORDS:* Lagrangian data assimilation, data assimilation, drifter assimilation, ocean prediction, ocean modeling

**Citation:** Özgökmen, T. M., A. Molcard, T. M. Chin, L. I. Piterbarg, and A. Griffa, Assimilation of drifter observations in primitive equation models of midlatitude ocean circulation, *J. Geophys. Res.*, 108(C7), 3238, doi:10.1029/2002JC001719, 2003.

### 1. Introduction

[2] Lagrangian instruments play an essential role in our ocean observing system. They provide a good measurement of the horizontal motion of ideal water particles, at least in the mesoscale range [e.g., Davis, 1991]. Consequently, they are a valuable tool for the study of the ocean general circulation and associated transport. In the last decade, deployment of drifting buoys has increased drastically and the data density is expected to increase further in the coming years [Mariano *et al.*, 2002]. Historically, Lagrangian data have been used primarily to compute statistical properties of the circulation, such as mean flow structure, second-order statistics, and transport properties [e.g., Davis, 1991; Owens, 1991; Swenson and Niiler, 1996; Bauer *et al.*, 1998; Lavender *et al.*, 2000; Poulain, 2001; Fratantoni,

2001; Zhang *et al.*, 2001]. Oceanic Lagrangian data have stimulated development of novel methods to address issues of mixing and transport using tools based on dynamical system theory [e.g., Wiggins, 1992; Poje and Haller, 1999; Coulliette and Wiggins, 2000; Kuznetsov *et al.*, 2002]. Lagrangian data are used in statistical modeling of particle motion [Thomson, 1986; Griffa *et al.*, 1995; Griffa, 1996; Falco *et al.*, 2000], in prediction studies based on assimilation of Lagrangian data into Lagrangian stochastic models [Özgökmen *et al.*, 2000, 2001; Castellari *et al.*, 2001; Piterbarg, 2001a] and dynamical models [Piterbarg and Özgökmen, 2002], and for estimating Eulerian velocity fields [Toner *et al.*, 2001a, 2001b].

[3] Given the increasing drifter data density and the cost of such observations, there is a major motivation to better utilize Lagrangian data by introducing new techniques. In light of recent advances in the realism of ocean general circulation models (OGCMs) [e.g., Smith *et al.*, 2000; Garraffo *et al.*, 2001; McClean *et al.*, 2002], assimilation of the information provided by Lagrangian instruments into OGCMs is an important, timely, and challenging research problem with direct impact on the accuracy of ocean forecasting.

<sup>1</sup>Also at Consiglio Nazionale Delle Ricerche, IOF, La Spezia, Italy.

<sup>2</sup>Jet Propulsion Laboratory, California Institute of Technology, Pasadena, California, USA

[4] In this study, we focus on the treatment of upper ocean drifter position data for the correction of surface velocity field in OGCMs. The primary problem is posed by the nonlinear nature of the relationship between the path followed by the drifters leading to position information  $\mathbf{r}$  at selected sampling intervals  $\Delta t$ , and the underlying Eulerian flow field  $\mathbf{u}$ , which is a prognostic variable set in OGCMs. A simple and common solution to this problem is to approximate the Eulerian field by  $\Delta\mathbf{r}/\Delta t$ , and to assimilate this velocity estimate into OGCMs (the so-called ‘‘Pseudo-Lagrangian’’ assimilation) [e.g., *Hernandez et al.*, 1995; *Ishikawa et al.*, 1996]. This method works well provided that the sampling period is much shorter than the Lagrangian correlation timescale (the  $e$ -folding timescale of the Lagrangian autocorrelation function of turbulent velocities)  $T_L$ , or  $\Delta t \ll T_L$ . At the Global Drifter Center (NOAA Atlantic Oceanographic and Meteorological Laboratory, Miami), drifter positions data are posted at the interval of 6 hours, after data gaps of up to 3 days are removed by interpolation [*Hansen and Poulain*, 1996]. In comparison,  $T_L$  has a nominal range of 1 to 3 days for ocean surface and 7 to 14 days for subsurface flows [*Griffa*, 1996]. Given that in practice,  $\Delta t$  is not much smaller than  $T_L$ , there is a clear motivation for exploring alternative techniques for assimilation of drifter data in OGCMs.

[5] A technique to assimilate drifter trajectories using a variational adjoint method was developed by *Kamachi and O'Brien* [1995], and applied to a simple model of the equatorial Pacific Ocean. In the variational formalism, a cost function measuring the distance between the trajectories of the model simulated buoys and the observed buoys (either from twin experiments or real data) is minimized. This technique requires the integration of an adjoint model, which needs to be developed specifically for each ocean model. An interesting technique was put forth by *Mead and Bennett* [2001], who carried out variational data assimilation of Lagrangian data into an ocean model expressed in Lagrangian form. Therefore, one faces the question whether the number of drifters within the domain of interest and the benefits of assimilation are worth developing an adjoint model or reformulating the ocean model in Lagrangian coordinates and the associated computational cost. A simple, computationally efficient and portable approach was recently developed by *Molcard et al.* [2003] based on optimal interpolation method, which takes into account rigorously the Lagrangian nature of the observations. An idealized version of this general mathematical formulation is implemented in the framework of a reduced-gravity, quasi-geostrophic model of midlatitude double-gyre circulation. An extensive study is conducted using twin experiments to quantify the effectiveness of Lagrangian data assimilation as a function of the number of drifters, the frequency of assimilation and uncertainties associated with the forcing functions driving the ocean model. The performance of the Lagrangian assimilation technique is also compared to that of conventional methods of assimilating drifters as moving current meters, and assimilation of Eulerian data, such as fixed-point velocities. It is found that this technique performs significantly better than Pseudo-Lagrangian assimilation in the sampling regime  $(T_L/5) \leq \Delta t \leq (T_L/2)$ . For  $\Delta t \ll T_L$ , Lagrangian and Pseudo-Lagrangian assimilation methods are approximately equivalent, and for

$\Delta t \geq T_L$ , all methods fail to provide useful Eulerian information for the correction of the ocean model circulation field.

[6] The method by *Molcard et al.* [2003] was tested in a quasi-geostrophic model, which integrates vorticity as the only prognostic variable. Also, the variability of the flow field in quasi-geostrophic models is much less than that in primitive equation models due to various linearizations, leading to relatively smooth trajectories. Therefore, it is not known how this method will be transformed to and perform in primitive equation models, which integrate multiple prognostic variables, such as horizontal velocity components and layer thickness. Also, the advantages of Lagrangian assimilation technique with respect to Pseudo-Lagrangian assimilation are shown by *Molcard et al.* [2003] within the context of the same assimilation method. Hence it is not known how the Lagrangian assimilation scheme performs when compared to more sophisticated Pseudo-Lagrangian assimilation methods.

[7] The present study has two objectives: (1) to extend the Lagrangian assimilation method by *Molcard et al.* [2003] to primitive equation models, and (2) to quantify the performance of Lagrangian assimilation technique relative to a state-of-the-art Pseudo-Lagrangian assimilation method. Specifically, the Lagrangian assimilation method by *Molcard et al.* [2003] is extended to primitive equation case using a simple and computationally efficient technique which maintains a dynamical consistency between the velocity corrections calculated from position data and the corresponding corrections on the geopotential (layer thickness). The Lagrangian approach is then evaluated by comparison to Pseudo-Lagrangian assimilation methods including a Kalman filter implementation [*Chin et al.*, 1999] that employs a Pseudo-Lagrangian observation operator. A quantitative evaluation is made through a set of twin experiments using a midlatitude, reduced-gravity configuration of the Miami Isopycnic Coordinate Ocean Model (MICOM).

[8] The paper is organized as follows: In section 2, assimilation techniques are described in detail. The experimental setup is introduced in section 3. The results are presented in section 4. We conclude in section 5. Appendix A includes details on error analysis.

## 2. Assimilation Algorithms

[9] The position measurements provided by the drifters can be translated into velocity information using the Pseudo-Lagrangian or Lagrangian techniques discussed in detail by *Molcard et al.* [2003]. The velocity information must correct all prognostic variables of the model to ensure that the correction fields are dynamically consistent with the model physics [e.g., *Ghil and Malanotte-Rizzoli*, 1991]. Optimization techniques such as the Kalman filter and variational relaxation are used to maintain such dynamical consistency; however, these assimilation methods have high development and computational costs. In this section, we present an alternative technique that has much lower operational cost and, as we will see, is effective for assimilation of the drifter data. We first introduce the correction of layer thickness, in the context of the primitive equation model used here, corresponding to the assimilation of horizontal velocity

components. Then different assimilation procedures are presented.

### 2.1. Correction of Layer Thickness in a Primitive Equation Model

[10] The numerical model used in this study is MICOM, which is a primitive equation, layered model. MICOM is a comprehensive large-scale ocean model, which is well documented in the literature [e.g., Bleck *et al.*, 1992; Bleck and Chassignet, 1994]. Here a reduced-gravity version of this model is preferred for simplicity, because a multi-layer configuration requires implementation of specific assimilation techniques to project surface information along fluid depth [e.g., Chin *et al.*, 2002]. Multi-layer dynamics are not investigated here, and will be subject of a future investigation.

[11] In the reduced-gravity configuration, the model integrates the following momentum and layer-thickness conservation equations:

$$\frac{\partial u}{\partial t} + \mathbf{u} \cdot \nabla u - f, v = -g' \frac{\partial h}{\partial x} + \rho^{-1} \frac{\partial \tau^x}{\partial z} + \nu_H h^{-1} \nabla \cdot h \nabla u, \quad (1)$$

$$\frac{\partial v}{\partial t} + \mathbf{u} \cdot \nabla v + f u = -g' \frac{\partial h}{\partial y} + \rho^{-1} \frac{\partial \tau^y}{\partial z} + \nu_H h^{-1} \nabla \cdot h \nabla v, \quad (2)$$

$$\frac{\partial h}{\partial t} + \nabla \cdot (\mathbf{u}h) = 0, \quad (3)$$

where  $\mathbf{u} = (u, v)$  is the layer-averaged horizontal velocity vector,  $h$  is the thickness of a layer of constant density,  $g' = g \frac{\Delta \rho}{\rho}$  is the reduced gravity,  $g$  is gravitational acceleration,  $\rho$  is the layer density,  $\Delta \rho$  is the density difference between the active and motionless layers,  $f = f_0 + \beta_0 v$  is the Coriolis frequency with beta-plane approximation,  $\boldsymbol{\tau} = (\tau^x, \tau^y)$  is the wind stress vector, and  $\nu_H$  is the lateral viscosity coefficient.

[12] Given the velocity corrections  $(\Delta u, \Delta v)$  derived from the drifter data, we wish to find the layer thickness correction  $\Delta h$ , that satisfies the momentum equations approximately. The momentum equations (1) and (2) are rewritten to emphasize the geostrophic momentum balance as

$$T^x - f \Delta v = -g' \frac{\partial(\Delta h)}{\partial x}$$

$$T^y + f \Delta u = -g' \frac{\partial(\Delta h)}{\partial y},$$

where  $T^x$  and  $T^y$  denote the ageostrophic momentum terms in each direction, which consist of accelerations due to time dependence, nonlinearity, forcing, and dissipation. The correction to the layer thickness due to corrections to velocity components can then be calculated from

$$\nabla^2(\Delta h) = \frac{1}{g'} \left[ f \frac{\partial(\Delta v)}{\partial x} - f \frac{\partial(\Delta u)}{\partial y} - \beta_0 \Delta u - \frac{\partial T^x}{\partial x} - \frac{\partial T^y}{\partial y} \right].$$

The last two terms on the rhs of the above equation require the calculation of ageostrophic momentum terms, which is

generally computationally cumbersome, and not done here. Omission of these terms restricts the validity of layer correction to midlatitude ocean circulation. The term in the middle scales with respect to the first two as  $(\beta_0 L)/f_0$ , where  $L$  is the scale of gradients, for example, the eddy scale. For midlatitudes,  $\beta_0 = 2 \times 10^{-11} m^{-1} s^{-1}$ ,  $L \approx 2 \times 10^5 m$ ,  $f_0 = 10^{-4} s^{-1}$ , and  $(\beta_0 L)/f_0 \ll 1$ ; hence this term is neglected as well. Therefore we are left with a simple equation, which calculates the correction to layer thickness from geostrophic balance

$$\nabla^2(\Delta h_g) = \frac{f}{g'} \left[ \frac{\partial(\Delta v)}{\partial x} - \frac{\partial(\Delta u)}{\partial y} \right], \quad (4)$$

subject to homogeneous boundary conditions  $\Delta h_g = 0$  to ensure that  $\Delta h_g \rightarrow 0$  as  $\Delta u$  and  $\Delta v \rightarrow 0$ ; that is, in the absence of any corrections to velocity field from drifter data, there is no correction to layer thickness field. Computationally, equation (4) is solved by a fast Fourier transform technique.

[13] We next consider a formulation of constraint imposed by the continuity equation of the model, which is an expression for mass conservation. It is important to note that the correction to the layer thickness is a function of the correctional velocity field, which in turn depends on the data distribution. Let us assume that the sampling is not homogeneous, but only several anticyclonic eddies are sampled. In this case, the tendency from equation (4) will be to increase the layer thickness at the eddy locations, which in effect adds mass to the layer. However, this is only an artifact of sampling, and there is no physical reason for the layer mass to change in the absence of explicit incorporation of physical processes such as heating, evaporation, mixing, etc. Hence we calculate the net mass deviation induced by equation (4),

$$\Delta m = \frac{1}{|A|} \int_A \Delta h_g dA,$$

where  $A$  is the considered ocean basin and  $|A|$  its area, and adjust the final correction to conserve layer mass in the integrated sense

$$\Delta h = \Delta h_g - \Delta m. \quad (5)$$

Then the assimilation formula for the layer thickness becomes (see equation (A1))

$$h^a(n) = h^b(n) + \Delta h. \quad (6)$$

where the superscripts  $a$  and  $b$  denote ‘‘assimilated (data updated)’’ and ‘‘background (model predicted)’’ fields, respectively.

### 2.2. Lagrangian Assimilation Algorithm

[14] We assume that the data to be assimilated in a model is an array of  $M$  Lagrangian trajectories observed with some errors at time instances  $n\Delta t$ ,  $n = 1, 2, \dots, N$ . Denote the observations by  $\mathbf{r}_m^o(n)$  and the corresponding quantities obtained from the model by  $\mathbf{r}_m^b(n)$ , where the subscript stands for the drifter label. Let

$$\mathbf{v}_m^o(n) = \frac{\mathbf{r}_m^o(n) - \mathbf{r}_m^o(n-1)}{\Delta t} \quad \text{and} \quad \mathbf{v}_m^b(n) = \frac{\mathbf{r}_m^b(n) - \mathbf{r}_m^b(n-1)}{\Delta t}$$

denote the finite difference Lagrangian velocity obtained from the position increments for observations and model (tracer simulation), respectively. Also, let  $\mathbf{u}_{ij}(n) = \mathbf{u}(n\Delta t, i\Delta r, j\Delta r)$  be the Eulerian velocity values on a grid with scale  $\Delta r$  at time  $n$ . In our companion paper [Molcard et al., 2003], the assimilation formulas for velocity components based on optimal interpolation (OI) [e.g., Lorenc, 1986] have been derived as

$$\mathbf{u}_{ij}^a(n) = \mathbf{u}_{ij}^b(n) + \Delta\mathbf{u}_{ij}, \quad \Delta\mathbf{u}_{ij} = \beta \sum_{m=1}^M \gamma_{ijm} (\mathbf{v}_m^o(n) - \mathbf{v}_m^b(n)), \quad (7)$$

with the assimilation parameters (“influence function”) given as

$$\gamma_{ijm} = \exp\left(-\frac{(x_m^b(n) - i\Delta r)^2 + (y_m^b(n) - j\Delta r)^2}{2\Delta r^2}\right), \quad \beta = \frac{\sigma_b^2}{\sigma_o^2 + \sigma_b^2}, \quad (8)$$

where  $(x_m^b(n), y_m^b(n)) = \mathbf{r}_m^b(n)$ ,  $\sigma_b^2$  is the modeling velocity mean square error, and  $\sigma_o^2$  is the error for the Lagrangian velocity which is related to the error of independent positions, say  $\sigma_r^2$ , by  $\sigma_o^2 \sim \sigma_r^2/\Delta t^2$ . The derivation is based on two main assumptions: First, the velocity spatial gradients are small comparing to  $1/\Delta t$  and, second, the errors are uncorrelated in time and space [Molcard et al., 2003].

[15] After the velocity correction fields,  $\Delta\mathbf{u} = (\Delta u, \Delta v)$ , have been computed as equation (7), the corresponding changes to the layer thickness field are made according to the multivariate dynamic balancing (equations (4)–(8)) described earlier. We refer to this assimilation scheme as OI-Lag in the rest of the paper.

### 2.3. Pseudo-Lagrangian Assimilation Algorithms

[16] In Pseudo-Lagrangian assimilation, trajectories and Lagrangian velocities are not computed using the model, but rather the model Eulerian velocity is directly used to compute  $\Delta\mathbf{u}$ . In this study, we consider two algorithms for implementation of Pseudo-Lagrangian assimilation. The first one uses the same basic OI formulation as described above (called OI-PsLag), and the second one is based on a Kalman filter (called KF-PsLag).

#### 2.3.1. Pseudo-Lagrangian Optimal Interpolation OI-PsLag

[17] The Pseudo-Lagrangian formulation is simpler than the fully Lagrangian formulation, since there is no need to compute drifter position increments  $\Delta\mathbf{r}$  and Lagrangian velocity  $\mathbf{v}^b$  using the model. The observational operator is linear, and the difference between the observed Lagrangian velocity  $\mathbf{v}^o$  and the Eulerian model velocity  $\mathbf{u}^b$  appears directly in the correction term in equation (7), or explicitly,

$$\tilde{\mathbf{u}}_{ij}^a(n) = \mathbf{u}_{ij}^b(n) + \beta \sum_{m=1}^M \gamma_{ijm} \cdot (\mathbf{v}_m^o(n) - \mathbf{u}_m^b(n)), \quad (9)$$

where

$$\mathbf{u}_m^b(n) \approx \mathbf{u}^b(n\Delta t, \mathbf{r}_m(n\Delta t))$$

is the Eulerian velocity at the drifter position found by interpolating grid velocities. The correction of the layer thickness is carried out according to equations (4), (5), and (6) described in section 2.1.

#### 2.3.2. Pseudo-Lagrangian Kalman Filter KF-PsLag

[18] The Kalman filter is a statistically optimal interpolator that sequentially corrects for the data-prediction discrepancies, while dynamically updating the covariance field in a way compatible with the primitive equation model (MICOM) dynamics. In essence, the filter is designed to produce a dynamically optimal set of the assimilation parameters  $\beta\gamma_{ijm}$  in equation (9) given the model equations, the measurements from the past up to present, and assigned statistical accuracy (error covariances) in these dynamic model and measurements. A Kalman filter version of the Pseudo-Lagrangian method would serve as a benchmark for our proposed, simple dynamic adjustment technique described in section 2.1 (at least within an operating range relevant to the Global Drifter Center data set). It can also be used as a reference to determine the effects of the simple Lagrangian formulation (Lag-OI) for drifter assimilation. A combined implementation of the Lagrangian method and a Kalman filter is deferred as a future study, due to the highly nonlinear (and nonsequential) operations imposed by the Lagrangian technique.

[19] Owing to the number of variables, the Kalman filter algorithm must be approximated (usually by parameterization of the large covariance matrix) to be practical for data assimilation purposes in present-day computers. The particular realization used here, called “reduced-order information filter” (ROIF), has been demonstrated effective in reconstruction of mesoscale features in MICOM, as detailed by Chin et al. [1999, 2002].

### 2.4. Computational Issues

[20] While drifters provide data coverage over a large area, the total number of simultaneous drifters is likely to be small with respect to other assimilated observations (e.g., sea surface height, sea surface temperature) in the area of interest, and even in the entire ocean basin. Therefore it is important that algorithms to assimilate drifter positions are simple, portable, easy to implement, and computationally efficient. It is from this perspective that the effort in the present investigation is to be viewed.

[21] For some rough estimates, let us assume that  $K = O(10^4)$  is the number of model grid points,  $M = O(10^2)$  is number of assimilated drifters, and  $N = O(10^2)$  is the number of model time steps within each data assimilation period (see sections 3.1 and 3.4 for justification of the range of parameters). For the optimal interpolation (equations (7) and (8)) of the velocity data, the number of operations (multiplications) during a run is roughly  $O(KM) = O(10^6)$ . For the calculation of layer thickness correction, the inversion of the Laplacian operator in equation (4) can be performed using a Fourier-based fast algorithm with  $K\log_2 K \approx 10^5$  operations, and equation (5) needs  $O(K) = O(10^4)$  operations, both of which are as computationally efficient as the main assimilation formula. Finally, the additional particle advection routine for the Lagrangian scheme requires  $O(MN) = O(10^4)$  operations.

[22] Overall, the assimilation technique given by equations (4)–(8) offers significant computational gains over

**Table 1.** Parameters of the Numerical Ocean Model Simulations

Parameter	Value
Zonal basin size	$L_x = 2000$ km
Meridional basin size	$L_y = 2000$ km
Horizontal grid scale	$\Delta x = \Delta y = 20$ km
Coriolis parameters	$f_0 = 9.3 \times 10^{-5} \text{ s}^{-1}$ $\beta_0 = 2 \times 10^{-11} \text{ m}^{-1} \text{ s}^{-1}$
Layer thickness	$H = 1000$ m
Reduced gravity	$g' = 0.02 \text{ m s}^{-2}$
Deformation radius	$R_d = 42$ km
Wind stress amplitude	$\tau_0 = 0.1 \text{ Nm}^{-1}$
Lateral viscosity	$\nu_H = 400 \text{ m}^2 \text{ s}^{-1}$
Time step	$\delta t = 1200$ s

more comprehensive schemes, albeit at the expense of higher accuracy provided by the dynamical estimation of model and observation error covariances. As shown below, the assimilation scheme is effective in the absolute sense for assimilation of drifter data.

### 3. Experimental Setup

[23] Our experimental setup consists of configurations of the circulation model and of identical twin experiments, and determination of the parameter range for a systematic evaluation of results.

#### 3.1. Configuration of the Numerical Model

[24] The ocean model is set up in an idealized, large-scale configuration; the model is configured in a square domain of  $2000 \text{ km} \times 2000 \text{ km}$  and centered at  $30^\circ\text{N}$ . The equilibrium layer thickness is taken as  $1000 \text{ m}$ , and the stratification is such that the Rossby radius of deformation is approximately  $42 \text{ km}$ , typical of midlatitude circulation. The grid scale is  $20 \text{ km}$ , which is adequate for eddy-resolving simulations. The eddy viscosity coefficient is taken as  $\nu_H = 400 \text{ m}^2 \text{ s}^{-1}$  such that the viscous boundary layer scale  $(\nu_H/\beta_0)^{1/3} \approx 27 \text{ km}$  is larger than the grid spacing to ensure numerical stability. No-normal flow and no-slip

conditions are applied along all boundaries. The model is purely wind-driven (without thermodynamics) by a steady zonal wind stress of the form  $\tau^x = -\tau_0 \sin(\pi y/L_y)$ , where  $L_y$  is the meridional extent of the basin and  $y$  is the distance from the center of the domain. Hence the wind forcing drives a classic double-gyre circulation [Holland, 1978], traditionally used in studies of the complex interaction between dynamically-different regimes consisting of Sverdrup gyres, western boundary currents, midlatitude jet, and mesoscale eddies. The parameters of the numerical model are summarized in Table 1.

#### 3.2. Twin Experiments

[25] For a controlled comparison of the three assimilation techniques, OI-Lag, OI-PsLag, and KF-PsLag, an identical twin experiment approach is adopted (Figure 1). In the first experiment (CONTROL), MICOM is integrated until the model kinetic energy reaches a statistically steady state, and the circulation characterizing the double-gyre flow is attained, which requires approximately 10 years of spin-up period. Then, synthetic drifters are released in the CONTROL flow field, and are integrated using a fourth-order Runge-Kutta method. Hence synthetic drifters serve as ocean data. The position data are assimilated into a second model run (ASSIM), which is started from rest in order to eliminate the need for testing a variety of arbitrary initial conditions different from that of CONTROL. The model configurations for the CONTROL and ASSIM runs are identical for simplicity. This assumption is clearly unrealistic when considering the case of assimilation of real ocean drifter data into OGCMs; however, the effect of parameter differences in twin experiments has been partially investigated by Molcard *et al.* [2003], and the assimilation has been found to perform well in all cases.

[26] The primary advantage of the twin experiment approach is that the underlying Eulerian flow field for the drifter data is exactly known, and the performance of each assimilation scheme can be quantified. As the performance

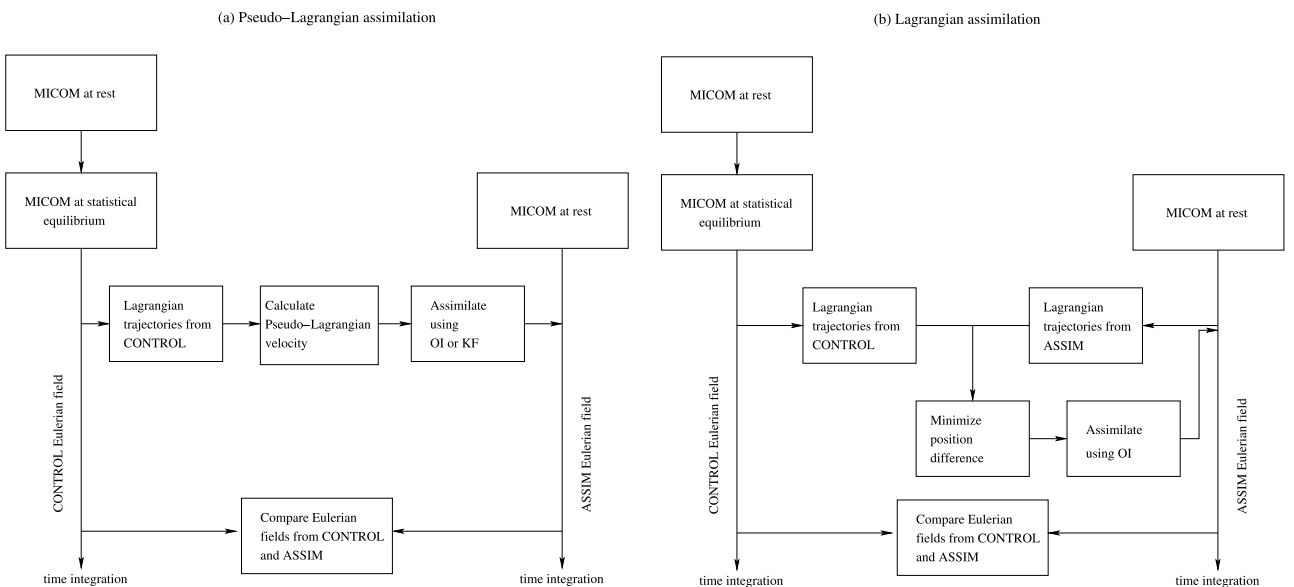


**Figure 1.** Schematic illustration of identical twin experiments using (a) Pseudo-Lagrangian and (b) Lagrangian assimilation.

metrics, we use the following normalized root-mean-squares of the velocity and layer thickness errors:

$$u_{error}(t) = \frac{\sqrt{\sum_{i,j}^K \left[ \left( u_{ij}^C(t) - u_{ij}^A(t) \right)^2 + \left( v_{ij}^C(t) - v_{ij}^A(t) \right)^2 \right]}}{\sqrt{\sum_{i,j}^K \left( u_{ij}^C(t) + v_{ij}^C(t)^2 \right)}}$$

$$h_{error}(t) = \frac{\sqrt{\sum_{i,j}^K \left( h_{ij}^C(t) - h_{ij}^A(t) \right)^2}}{\sqrt{\sum_{i,j}^K \left( h_{ij}^C(t) - H \right)^2}},$$

where subscripts ‘‘C’’ and ‘‘A’’ stand for CONTROL and ASSIM, respectively, and  $H = 1000$  m is the background layer thickness.

### 3.3. Assimilation Methods

[27] Our main objective is to compare the Lagrangian (OI-Lag) and Pseudo-Lagrangian (OI-PsLag) assimilation strategies. Since the Kalman filter is a mathematically formal approach to data assimilation, KF-PsLag is used for comparison purposes to give us a benchmark in performance evaluation.

[28] The primary difference between the Pseudo-Lagrangian and Lagrangian techniques is schematically shown in Figure 1. In the Pseudo-Lagrangian assimilation, velocity approximated from drifter positions in the CONTROL experiment is assimilated directly into the ASSIM experiment (Figure 1a). In the Lagrangian technique, the assimilation acts to minimize the position difference of drifters from CONTROL and ASSIM (Figure 1b). Lagrangian assimilation is implemented the following way (Figure 2). Let’s assume that a drifter position from CONTROL experiment is observed at point (A) at time  $t_0$ , and at point (B) at  $t_0 + \Delta t$ . The model is forwarded in time from  $t_0$  to  $t_0 + \Delta t$ , providing a forecast of its own drifter path from point (A) at time  $t_0$  to point (C) at  $t_0 + \Delta t$ , leading to a position increment  $\Delta \mathbf{r}^b$ . The observations are available at discrete time intervals of  $\Delta t$ , whereas ASSIM drifter path is nearly continuous at intervals of  $\delta t$ . ASSIM drifters are launched every  $\Delta t$  at the positions of the observed drifter data. Lagrangian velocity is calculated from  $\mathbf{v}^b = \Delta \mathbf{r}^b / \Delta t$  and compared with the observed drifter velocity  $\mathbf{v}^o$  at  $t_0 + \Delta t$ . The model Eulerian velocity  $\mathbf{u}^b(t_0)$  is modified in the vicinity of point (A), as a function of the difference between forecast (C) and observations (B) using equation (7). The radius of influence is taken approximately as the Rossby radius of deformation. The modification of model velocity field by going backward in time by  $\Delta t$  (to  $t_0$ ) is an adjoint-model-like operation, while being simpler in implementation. The main concept here is that  $T_L$  represents the limit of Lagrangian predictability [e.g., Piterbarg, 2001b], and it is only necessary to consider drifter path history on the order  $T_L$ . Therefore, devising adjoint-like schemes to integrate backwards in time for longer periods than  $T_L$  will not necessarily provide a more useful information for the correction of the model Eulerian field. The modified ASSIM field then yields an updated drifter forecast (D),

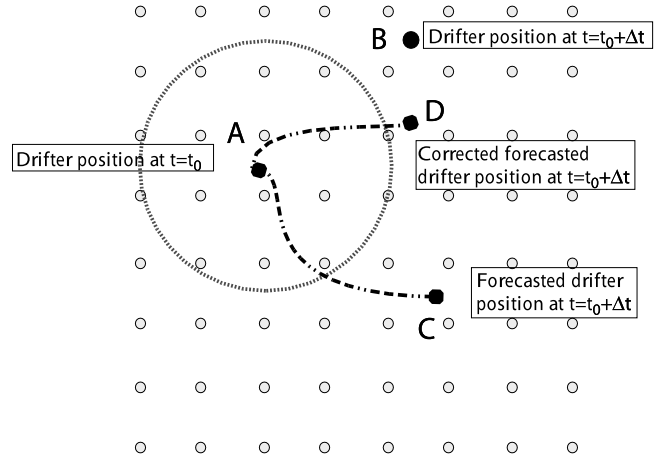


**Figure 2.** Schematic illustration of the assimilation algorithm. Given the drifter positions at  $t = t_0$  (A) and  $t = t_0 + \Delta t$  (B), the model forecast at  $t = t_0 + \Delta t$  is improved from (C) to (D) by modifying the model Eulerian circulation field at  $t = t_0$  within a circle of influence (model grid layout is shown in the background) using algorithm (7)–(8), which acts to minimize the distance between positions (B) and (C). The drifter position data are given at discrete time intervals  $\Delta t$ , whereas the model simulated drifters can follow paths as shown between forecasted and corrected positions, (A)–(C) and (A)–(D), respectively.

which is closer to the observed drifter arrival point (B) than the original forecast (C).

### 3.4. Observation Density

[29] The remaining important parameters of the twin experiments are the spatial and time sampling scales of drifter data. The drifters are homogeneously distributed over the entire domain in order to reduce or eliminate any dependence of results to initial launch locations. The reader is referred to Poje *et al.* [2002] for detailed considerations on drifter launch strategies. Three different spatial densities are selected: 36 drifters ( $6 \times 6$ ), which is the minimum density at which results are approximately insensitive to the initial locations; 121 drifters ( $11 \times 11$ ), which is the density above which results are not only approximately insensitive to the number of drifters, but are also oceanographically not feasible; and 64 drifters ( $8 \times 8$ ), which is an intermediate density between the two others. In order to constrain the time sampling parameter, or assimilation period  $\Delta t$ , Lagrangian decorrelation timescale  $T_L$  is estimated by dividing the domain into nine quasi-homogeneous, equal partitions, and by calculating Lagrangian autocovariance functions of the fluctuation velocities from drifter data in each regime. As expected, turbulent kinetic energy is highest in the midlatitude jet region, leading to  $T_L \approx 6$  days (Figure 3a), and fluctuation energy is much lower in the interior gyres, with  $T_L \approx 30$  days (Figure 3b). The assimilation period should be less than the smallest  $T_L$  for the assimilation schemes to be effective. Here we chose two assimilation frequencies:  $\Delta t = 6$  hours ( $\ll T_L$ ), which corresponds to the official sampling of drifter data available from the Global Drifter Center, and  $\Delta t = 3$  days, which is representative of typical data gaps existing in, for instance,

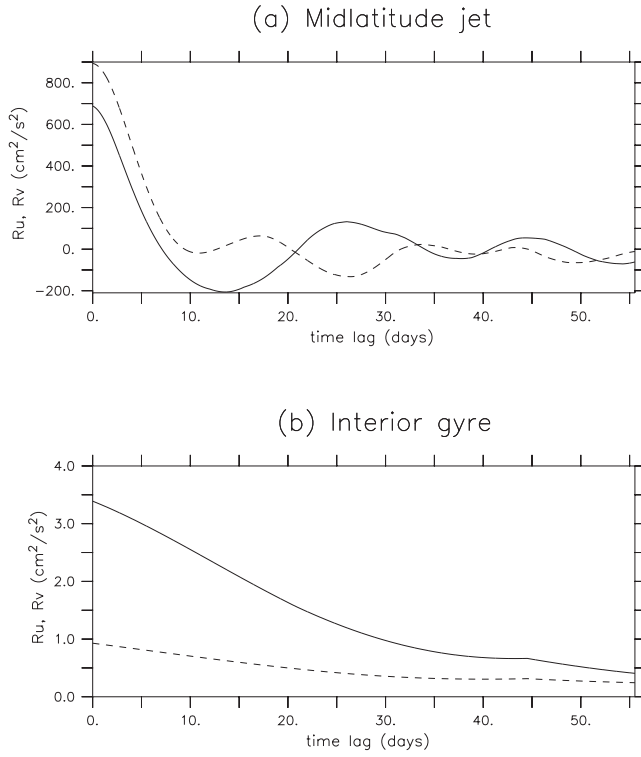


**Figure 3.** Lagrangian autocovariance functions of the fluctuation velocities for (a) meandering jet region and (b) interior gyre region. The solid (dashed) line shows the meridional (zonal) component.

WOCE (World Ocean Circulation Experiment) drifter data, and corresponds to approximately half of the minimum  $T_L$  in the modeled circulation. The total assimilation period is 360 days, which is found to be adequate to characterize the error convergence of the assimilation experiments. Parameters of assimilation methods are shown in Table 2.

## 4. Results

[30] First, results from experiments with 18 different parameters, i.e., resulting from three assimilation methods (OI-Lag, OI-PsLag, and KF-PsLag), three spatial sampling densities (36, 64, 121 drifters), two time sampling periods ( $\Delta t = 6$  hours,  $\Delta t = 3$  days), are presented. Then, the impact of the dynamical correction of  $h$  via (4–6) on the assimilation performance is discussed.

### 4.1. Comparison of Assimilation Methods

[31] The typical evolution of the identical twin experiments is shown in Figures 4 and 5 for the case of assimilation using OI-Lag with  $\Delta t = 6$  hours and 64 drifters. Drifters are initially uniformly distributed in the domain and are advected with the fully-developed CONTROL model field, while being assimilated into ASSIM, which is started from rest. A comparison of interface displacement fields,  $[h(x, y, t) - H]$  shows that after 10 days of assimilation, drifters in the high-energy jet region already exhibit an effect in ASSIM with major features taking shape, while being weaker and inaccurate in comparison to CONTROL (Figures 4a, 4b, and 4c). However, at 30 days of assimila-

tion, there is already a good agreement between ASSIM and CONTROL (Figures 4d, 4e, and 4f), while at 90 days of assimilation, they are virtually indistinguishable (Figures 4g, 4h, and 4i). The comparison of CONTROL and ASSIM velocity fields is shown in Figure 5, which follows the above description as well. Note that the development of the circulation requires multiple crossings of Rossby waves across the basin to form the western boundary currents, which in turn generate the midlatitude jet and eddies, following approximately 10 years of integration. In the absence of assimilation, the model only exhibits early stages of wind-driven spinup at  $t = 90$  days (Figure 6) and is far from the state of the CONTROL (Figures 4h and 5h). The primary point is that all experiments considered here have a similar evolution, and a visual evaluation of results in a qualitative sense is not feasible. Therefore the results are presented using quantitative error plots. It is also found that there is no significant difference between  $h_{error}$  and  $v_{error}$  in terms of differentiating the performance of the assimilation schemes. Hence only  $h_{error}(t)$  is employed in the following.

[32] An important consideration is that the use of a single realization may not be adequate for a quantitative intercomparison. Therefore, multiple realizations are conducted by starting the CONTROL simulation from different initial conditions (each 180 days or 360 days apart to ensure total statistical decorrelation), and ASSIM from rest, and the average of the resulting error curves are presented. It is found that three and five realizations are adequate for the nine different experiments with  $\Delta t = 6$  hours and  $\Delta t = 3$  days, respectively. As shown below, experiments with  $\Delta t = 6$  hours exhibit small variability; hence a smaller number of realizations is adequate. Overall, results based on 72 assimilation experiments are presented. Given the computational requirements of integrating twin models, drifters, and assimilation, a higher number of experiments does not appear to be feasible nor necessary.

[33] Evolutions of layer thickness error  $h_{error}(t)$  are shown in Figure 7. The plots are grouped by the assimilation frequency ( $\Delta t = 6$  hours: a, b, c and  $\Delta t = 3$  days: d, e, f) and the number of drifters, so that the three different assimilation techniques are compared in each plot. When  $\Delta t$  is small, the differences between assimilation methods are also small, as expected. The initial convergence rate and the error values at the end of 360 days of assimilation are only a function of drifter density; as the drifter density increases, the initial rate of error decay increases, and the final error value decreases similarly for all methods, OI-Lag, OI-PsLag, and KF-PsLag (Figures 7a, 7b, and 7c). On the other hand, when  $\Delta t$  is larger, or when  $\Delta t = 3$  days  $\approx (T_L)_{min}/2$ , we expect differences between Pseudo-Lagrangian and Lagrangian, and also between OI and more sophisticated KF methods. In this case, the performance of KF-PsLag is better than that of OI-PsLag, and OI-Lag appears to lead to

**Table 2.** Parameters of the Assimilation Methods OI-Lag and OI-PsLag

Parameter	Value
Number of drifters	36 or 64 or 121
Assimilation period	$\Delta t = 21,600$ s or $\Delta t = 259,200$ s
Observation and model error ratio	$(\sigma_o/\sigma_b)^2 = 10^5$ s <sup>2</sup>
Radius of area of influence	50–70 km

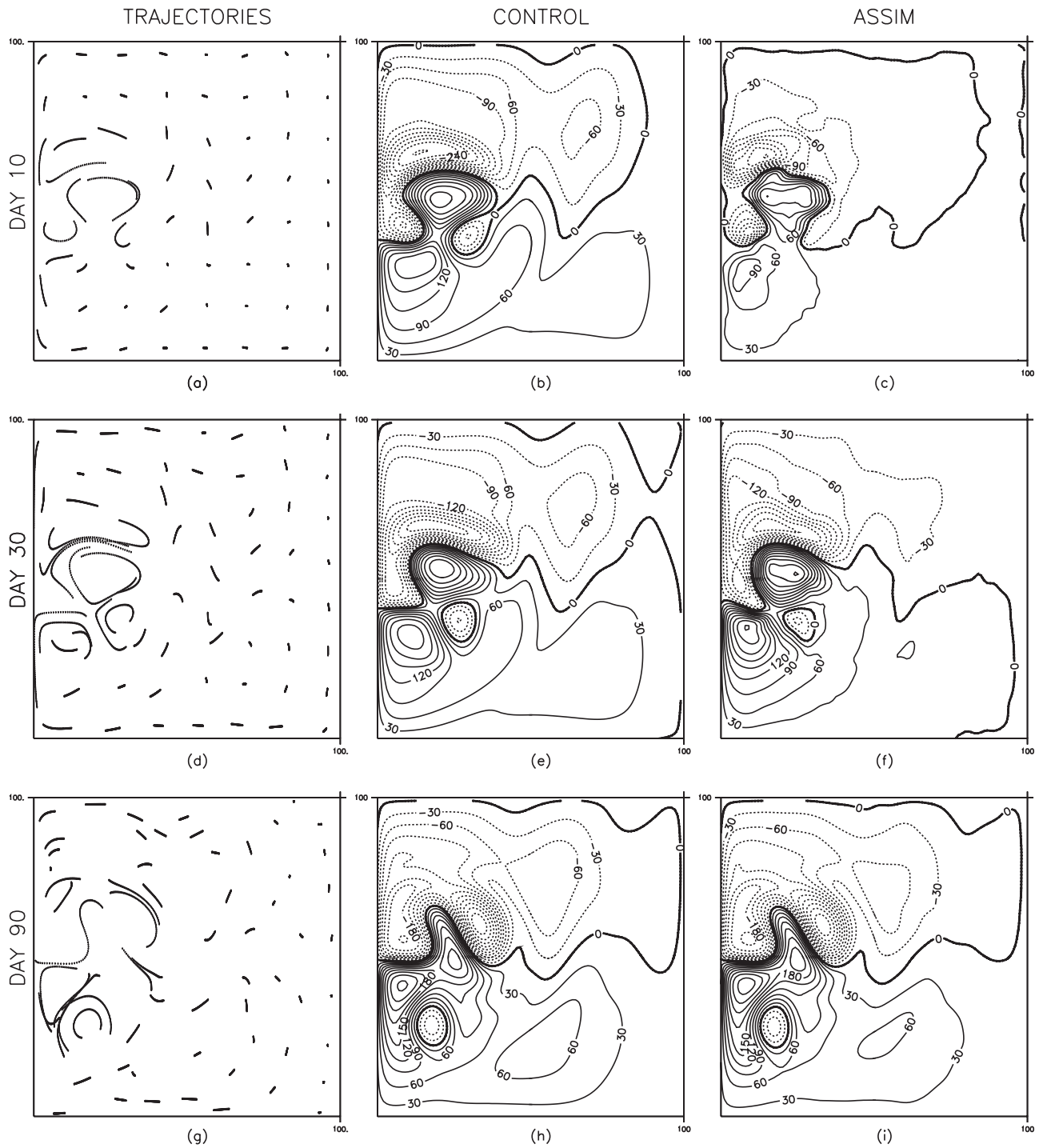


**Figure 4.** (a, d, g) Drifter trajectories and interface displacement [ $h - H$ ] (contour interval: 30 m) for (b, e, h) the control and (c, f, i) assimilation ocean model fields at selected times ( $t = 10$  days,  $t = 30$  days,  $t = 90$  days) of assimilation using OI-Lag for the case of  $\Delta t = 6$  hours and 64 drifters. Trajectories are shown for 10 days in Figure 4a and for the last 20 days in Figures 4d and 4g. Note the rapid convergence of ASSIM to CONTROL.

improved results with respect to both (Figures 7d, 7e, and 7f). Also, errors corresponding to each drifter density level deteriorate for  $\Delta t = 3$  days when compared to those for  $\Delta t = 6$  hours, as expected.

[34] It also appears from Figures 7d, 7e, and 7f that all techniques exhibit a nearly-exponential convergence.

In order to confirm this observation,  $\ln(h_{error})$  is plotted linearly in time for all techniques in the case of 64 drifters (others show a similar behavior). Figure 8 indicates that the convergence of ASSIM to CONTROL can be characterized in three stages, which exhibit piecewise and nearly-constant slopes (or exponential convergence). In the initial stage

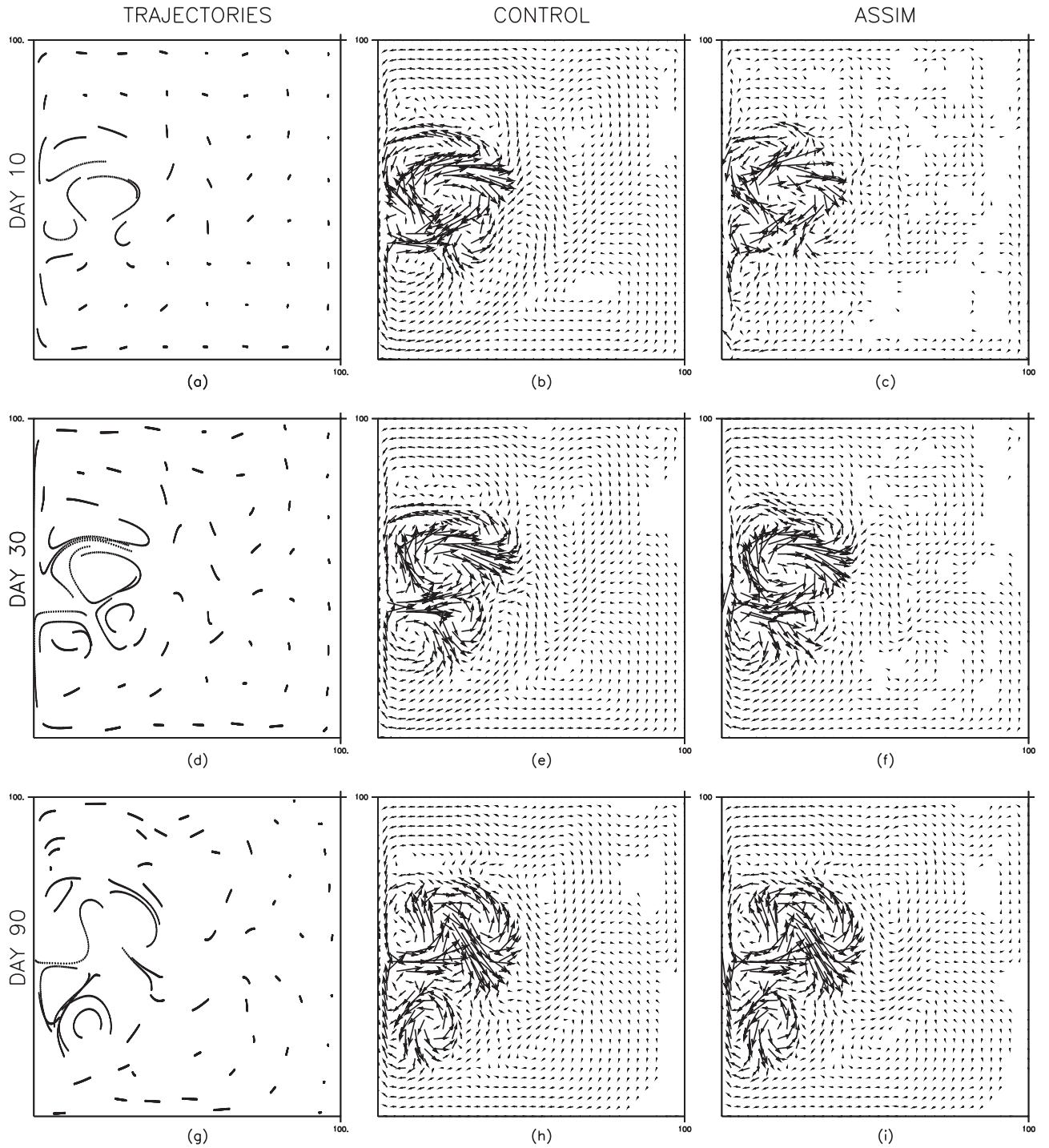


**Figure 5.** Same as in Figure 4, but for the ocean model velocity field  $\mathbf{u}$ . One out of three velocity vectors in each direction is shown. The maximum velocity magnitude is approximately  $1 \text{ m s}^{-1}$ .

( $0 \leq t < 60$  days), all methods show an exponential decay in error, and the rate of decay reduces somewhat in the intermediate stage ( $60 \leq t \leq 200$  days). Near the end of the integration ( $t > 200$  days), Pseudo-Lagrangian methods asymptote to a constant value, whereas OI-Lag continues to reduce the error at the same exponential rate. (However, the net reduction of error is small, as the error amplitude is small at this time.) As the major reduction of error takes place in

the first few months of assimilation for all techniques, all cases are simply approximated by

$$h_{error} \sim \exp\left(-\frac{t}{t_0}\right) + h_{error}^*,$$

where  $t_0$  is the  $e$ -folding timescale of error, calculated by estimating the slope of the lines (Figure 8) in the interval of

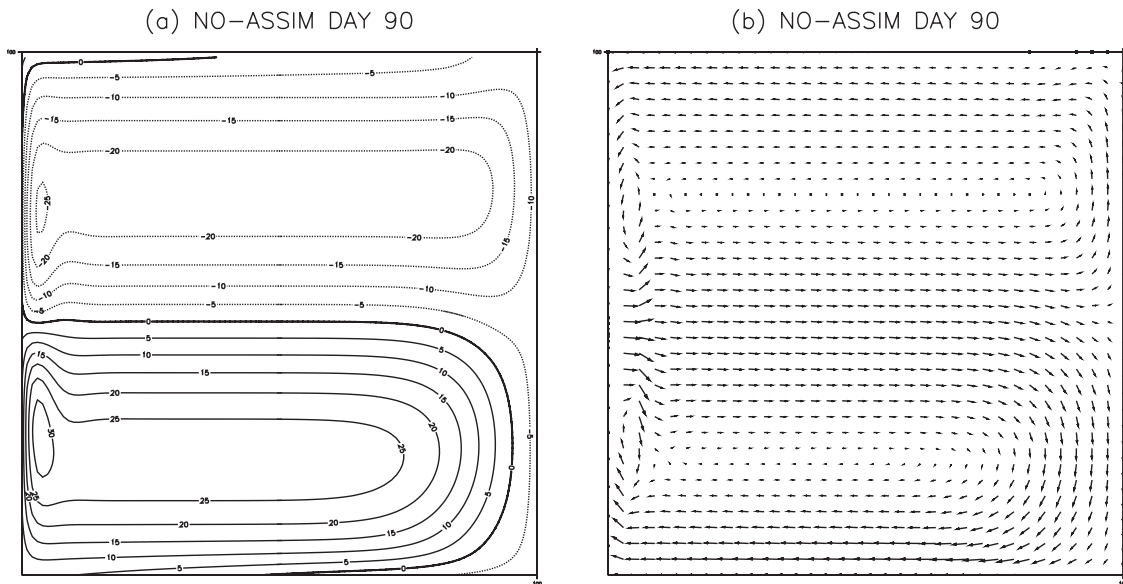


**Figure 6.** (a) Interface displacement (ci: 5 m) and (b) velocity field (maximum velocity vector amplitude  $\approx 0.17 \text{ m s}^{-1}$ ) at  $t = 90$  days in the experiment without the assimilation of drifter data.

$0 \leq t \leq 60$  days using a least-square fit, and  $h_{error}^*$  is the residual convergence error calculated in the interval  $300 d \leq t \leq 360$  days. Therefore,  $t_0$  and  $h_{error}^*$  serve as simple metrics to illustrate the differences between the three techniques. The results are shown in Figure 9 for all experiments with  $\Delta t = 3$  days. The comparison of the  $e$ -folding timescales (Figure 9a) indicates that  $t_0$  decreases as the number of drifters increases, at approximately the same rate for OI-Lag and OI-PsLag, and at a higher rate for KF-PsLag. The most notable aspect in Figure 9a is that OI-Lag using only 36 drifters yields equivalent performance (and much better with 121 drifters) as for OI-PsLag using 121 drifters. This demonstrates the improvement in performance due to Lagrangian technique. The impact of differences in  $t_0$  is then clearly reflected in  $h_{error}^*$  (Figure 9b). The residual errors for both OI methods reduce with increasing number of drifters, but they are in the range of 16–23% for OI-PsLag, whereas OI-Lag converges to a very low 0.5–4%. Residual errors for KF-PsLag are nearly constant at 10% and are relatively independent of the number of drifters. Overall, the implementation of the Lagrangian assimilation technique in an otherwise conventional OI method appears have improved significantly the convergence characteristics and accuracy of the method in the range where assimilation period is significant when compared to the minimum Lagrangian correlation time in the system.

#### 4.2. Impact of Dynamic Correction of Layer Thickness

[35] Experiments presented in section 4.1 clearly illustrate the effectiveness of the assimilation schemes, and in particular that of the Lagrangian technique, when applied to the primitive equation model. As outlined in section 2, our assimilation technique consists of two steps: first, the correction of the velocity field using Lagrangian data via equations (7) and (8), and second, the dynamical (geostrophic) correction to the layer thickness via equations (4)–(6). It is important to understand the impact of this second step, dynamical correction, on the performance of the assimilation. If the impact is found to be small, then the conclusion would be that this step is not very crucial, and

velocity/position information alone are adequate. On the other hand, if the impact is large, then it becomes very important how to bridge the gap to  $h$  correction when geostrophy doesn't hold (e.g., at low latitudes), when other information such as altimeter data are available, and when drifter information is obtained at different depths (at the surface, subsurface and deep ocean).

[36] In order to address this question, a number of experiments are conducted, in which drifter data are assimilated using only the velocity correction, and without simultaneously correcting the layer thickness. Here the results from OI-Lag with 121 drifters are shown, as this case is the least likely to show degradation of results due to sampling issues and inaccuracies of the method, and the change in accuracy results primarily from the missing  $h$ -correction. The results are illustrated for both  $\Delta t = 6$  hours and  $\Delta t = 3$  days cases in Figure 10. In both cases, the lack of  $h$ -correction has a significant impact leading to drastically slower response of the model to the assimilation. The greatest gain from  $h$ -correction is during the first 50 days, and  $h$ -correction has a bigger effect when  $\Delta t = 3$  days than when  $\Delta t = 6$  hours. The results are qualitatively similar for other drifter densities as well (not shown). This result not only supports the validity of the formulation (equations (4)–(6)) for the specific case considered in this study (midlatitude circulation, 1.5-layer model), but it also indicates that the correction of the model velocity field using drifters must be accompanied with an appropriate correction of the layer thickness field (or mass field, pressure, etc., depending on the model formulation) for such assimilation to be effective.

#### 4.3. Error Analysis

[37] Finally, analytical expressions of assimilation error are discussed. The ratio of Lagrangian and Pseudo-Lagrangian estimates was given for  $\beta \approx 1$  by Molcard *et al.* [2003],

$$r \equiv \frac{|\mathbf{u}_{ij}^a(n) - \mathbf{u}_{ij}(n)|}{|\tilde{\mathbf{u}}_{ij}^a(n) - \mathbf{u}_{ij}(n)|} \approx \frac{|\mathbf{D}_{ij}^b(n)\mathbf{u}_{ij}^b(n) - \mathbf{D}_{ij}^o(n)\mathbf{u}_{ij}^o(n)|}{|\mathbf{D}_{ij}^o(n)\mathbf{u}_{ij}^o(n)|}, \quad (10)$$

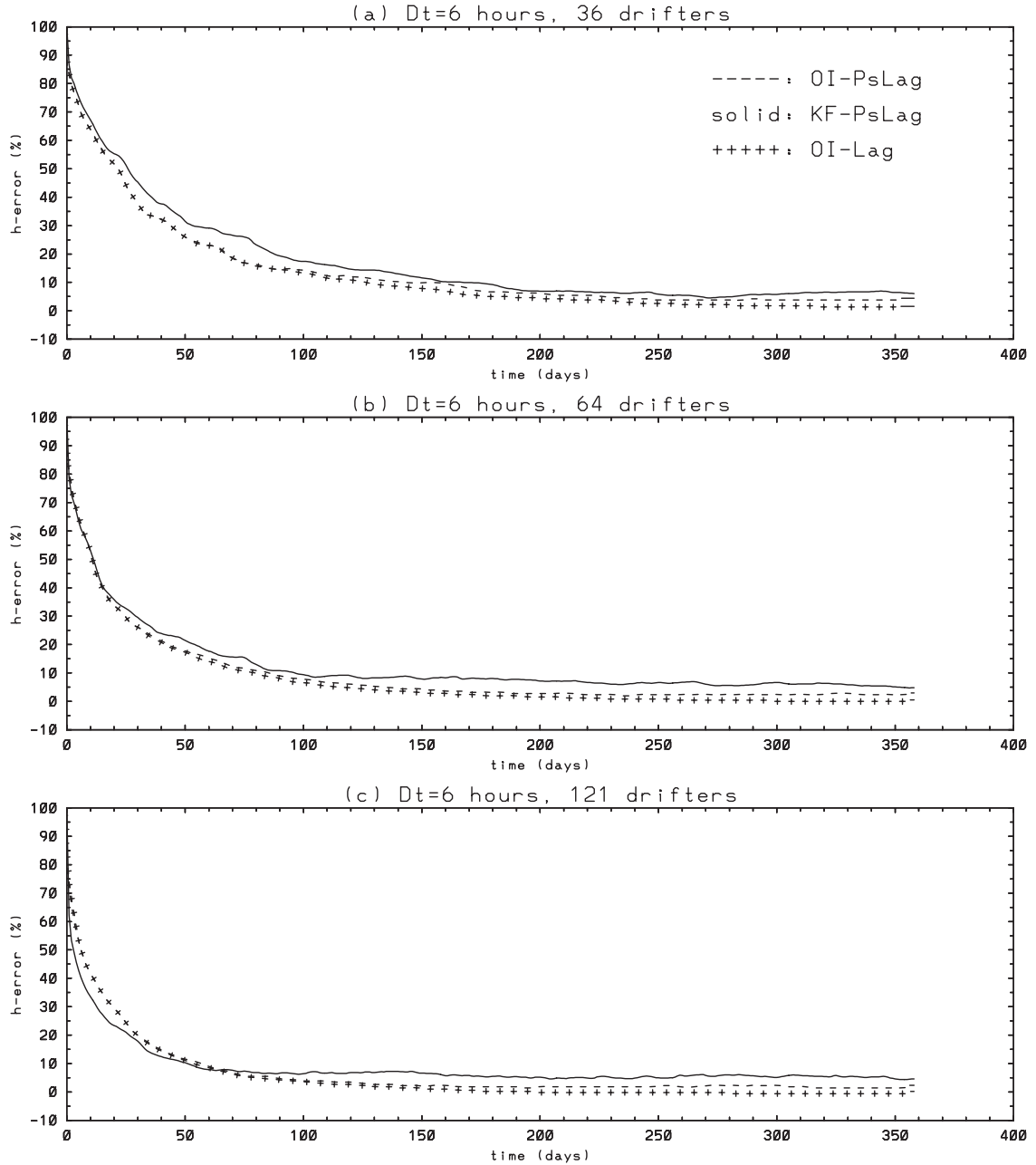


**Figure 7.** Average of layer thickness error  $h_{error}$  (in %) versus time (in days) from three realizations with  $\Delta t = 6$  hours and (a) 36 drifters, (b) 64 drifters, and (c) 121 drifters, and from five realizations with  $\Delta t = 3$  days and (d) 36 drifters, (e) 64 drifters, and (f) 121 drifters. Solid curves denote KF-PsLag, dashed curves denote OI-PsLag, and curves with pluses denote OI-Lag.

where

$$\mathbf{D}_{ij}(n) = \Delta t \begin{pmatrix} \partial u_{ij}(n)/\partial x & \partial u_{ij}(n)/\partial y \\ \partial v_{ij}(n)/\partial x & \partial v_{ij}(n)/\partial y \end{pmatrix}. \quad (11)$$

[38] The main objective here is to present and analyze an expression for the mean squared error (MSE) of assimilation procedure as a function of time and space sampling density,

and model and observation errors. The presented formula is designed for a qualitative analysis only and its derivation is given in Appendix A. Let

$$s_{ij}^2 = \left\langle \left( u_{ij}^a - u_{ij} \right)^2 + \left( v_{ij}^a - v_{ij} \right)^2 \right\rangle$$

be the absolute value of the error of velocity estimate (equation (7)) at the mesh  $(i, j)$  in a fixed moment, where  $u_{ij}$  and  $v_{ij}$  are the true velocity components and the angle

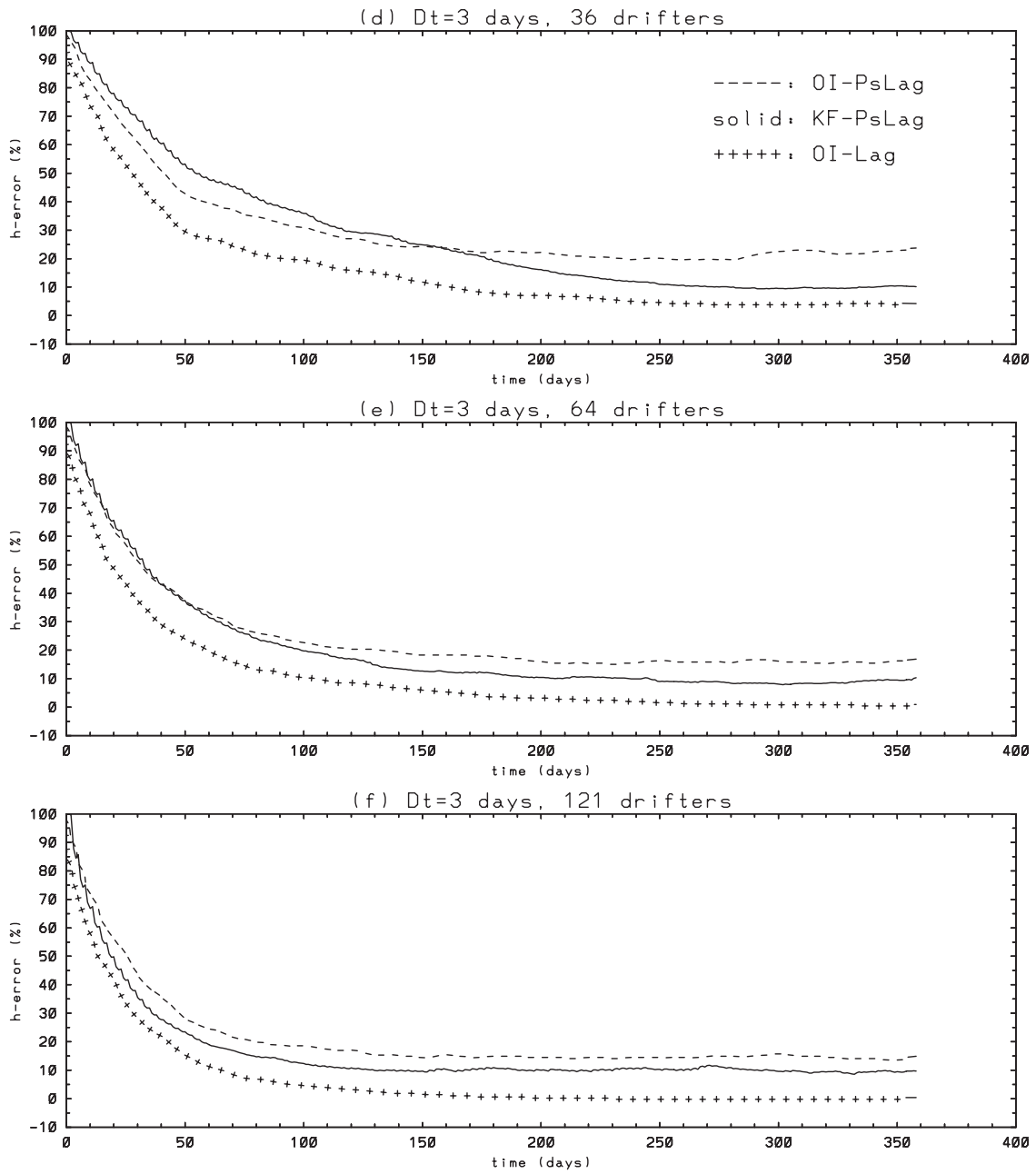


Figure 7. (continued)

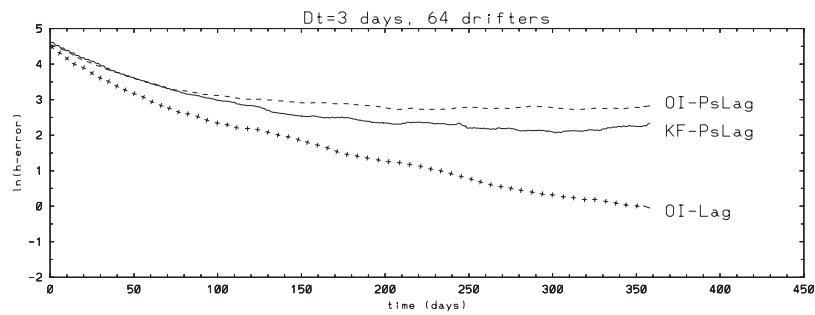
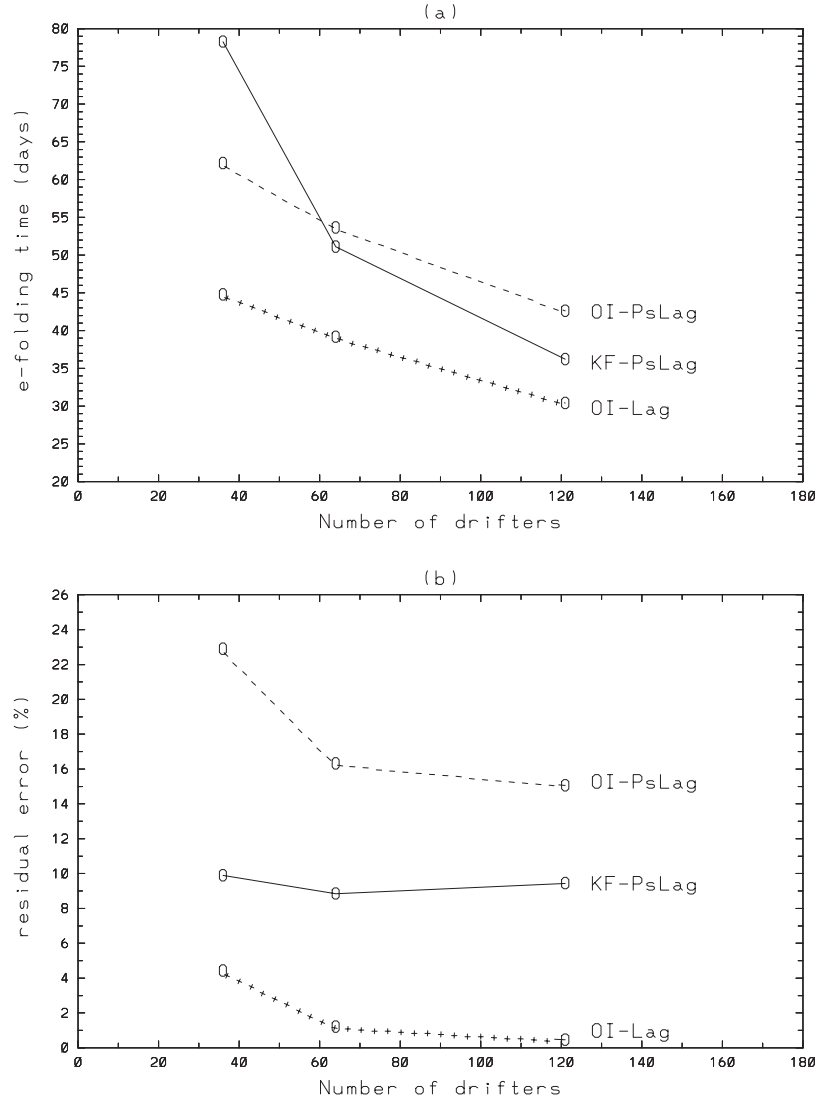


Figure 8. The  $\ln(h_{error})$  versus time in the case of  $\Delta t = 3$  days and 64 drifters for OI-PsLag, KF-PsLag, and OI-Lag.



**Figure 9.** (a) The  $e$ -folding timescales  $t_0$ , and (b) residual errors  $h_{error}^*$  as a function of the number of drifters and assimilation methods in the case of  $\Delta t = 3$  days.

brackets mean the expectation. Introduce the relative error averaged over the basin,

$$\delta_u^2 = \frac{\sum_{ij} s_{ij}^2}{\sum_{ij} (u_{ij}^2 + v_{ij}^2)}.$$

Then, arguments given in Appendix A show that

$$\delta_u^2 \sim \gamma(1 - \mu\beta(1 - \beta\varepsilon^2)), \quad (12)$$

and for the relative assimilation error of  $h$ ,

$$\delta_h^2 \leq \gamma(1 - \mu\beta(1 - \beta\varepsilon^2)). \quad (13)$$

Here

$$\gamma = \sigma_b^2 / u^2,$$

where  $u$  is a typical velocity magnitude at the region,  $\mu$  is the drifter density,  $\beta$  is defined in equation (8), and, finally,

$$\varepsilon = \frac{\Delta t}{2} \left\langle Sp \left( \frac{Du_{ij}^b}{Dr} \left( \frac{Du_{ij}^b}{Dr} \right)^T \right) \right\rangle^{1/2} \quad (14)$$

is a dimensionless parameter characterizing the observation frequency, where  $Sp(\mathbf{A})$  denotes the trace of matrix  $\mathbf{A}$ , and the velocity space gradient matrix is defined in equation (11). When deriving equation (12), we assumed that  $\varepsilon$  is small; that is, the observation frequency is high enough comparing to the velocity spatial gradients.

[39] We investigate whether equation (12) demonstrates a reasonable behavior in a typical parameter space. Consider drifter observation errors in the range  $10 \text{ m} \leq \sigma_r \leq 100 \text{ m}$  and modeling errors  $0.1 \text{ m s}^{-1} \leq \sigma_b \leq 0.5 \text{ m s}^{-1}$ . Their ratio is in the range  $4 \times 10^2 \text{ s}^2 \leq (\sigma_r / \sigma_b)^2 \leq 10^6 \text{ s}^2$ . For the time sampling densities used in this study,  $\Delta t = 21,600 \text{ s}$  and

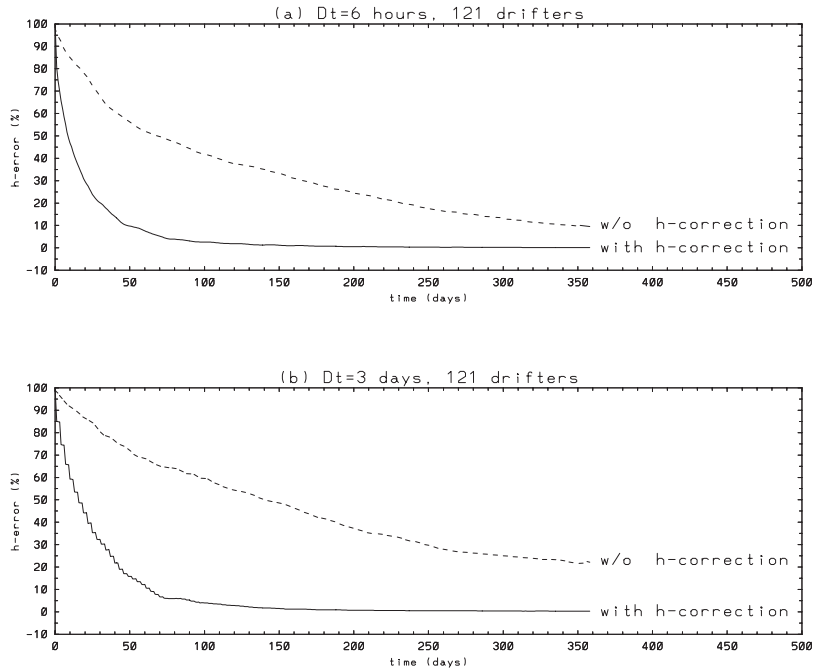


**Figure 10.** Layer thickness error  $h_{error}$  (in %) versus time (in days) with (solid curve) and without (dashed curve) the correction of layer thickness  $h$  in the case of 121 drifters and (a)  $\Delta t = 6$  hours and (b)  $\Delta t = 3$  days.

$\Delta t = 259,200$  s, we get  $0.998 \leq \beta < 1$  or  $\beta \approx 1$  for practical purposes. There are no solid indicators for  $\gamma$ , but based on the velocity range in the most energetic region  $0.1 \text{ m s}^{-1} \leq u_{ij} \leq 1.0 \text{ m s}^{-1}$ , let us assume that  $\gamma = 0.25$  or modeling error corresponds to 50% of typical velocity values. The error  $\delta_u$  from equation (12) is plotted for  $\beta = 1$  and  $\gamma = 0.25$  as a function of the nondimensional space sampling density parameter  $\mu$  and time sampling density parameter  $\varepsilon$  in Figure 11. If  $\varepsilon$  is interpreted as the ratio of sampling time and (minimum Eulerian/Lagrangian) velocity decorrelation timescale, then its range for the above experiments is  $0.04 \leq \varepsilon \leq 0.5$ . Also, as the ratio of the diameter of the influence area to grid scale was taken as approximately 7 for 36–121 drifters,  $0.15 \leq \mu \leq 0.6$ . Figure 11 illustrates that the relative error decreases as  $\mu$  increases and  $\varepsilon$  decreases, indicating convergence of the method as observation density increases. We note that in the limit that  $\mu \rightarrow 0$ ,  $\delta_u \rightarrow \sqrt{\gamma}$  or when there are no drifters, there is no correction with respect to the initial model error. Derivation of equation (12) is based on very restrictive assumptions and hence the given formula is not aimed at quantitative comparison with the experiments. Nevertheless, they give a good enough qualitative description of the error behavior which is in agreement with the experiments in this study.

## 5. Summary and Conclusions

[40] In light of recent advances in the realism of OGCMs [e.g., *Smith et al.*, 2000; *Garraffo et al.*, 2001; *McClean et al.*, 2002] and increasing density of drifter deployments in the ocean [*Mariano et al.*, 2002], assimilation of drifter observations in OGCMs emerges as an important, timely, and challenging research problem with a direct impact on ocean state forecasting. The primary objective of this study

is to extend the applicability of the Lagrangian assimilation method developed by *Molcard et al.* [2003] to more comprehensive OGCMs. In the context of a quasi-geostrophic model, *Molcard et al.* [2003] demonstrated that the Lagrangian method outperforms the conventional Pseudo-Lagrangian approach in the range  $(T_L/5) \leq \Delta t \leq (T_L/2)$ ,

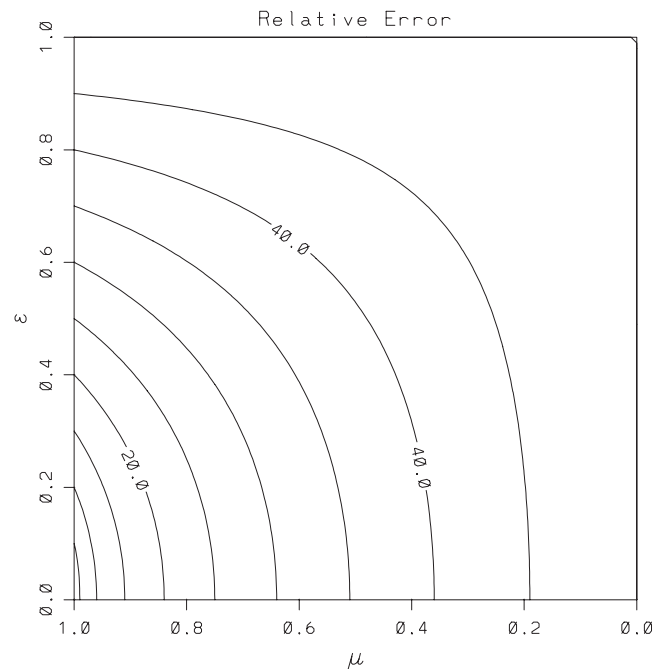


**Figure 11.** Relative error  $\delta_u$  ( $\geq \delta_h$ ) for  $\beta = 1$  and  $\gamma = 0.25$ , as a function of space sampling density parameter  $\mu$  and time sampling density parameter  $\varepsilon$  (contour interval: 5%).

which applies to many surface and subsurface oceanic drifter observations. (Also, for  $\Delta t \ll T_L$ , Lagrangian and Pseudo-Lagrangian assimilation methods are approximately equivalent, and for  $\Delta t \geq T_L$ , useful Eulerian information for the correction of the ocean model circulation field cannot be obtained for reasons of Lagrangian predictability limits). It is therefore desirable to implement such Lagrangian assimilation in primitive equation models as well. The main obstacle is that a single prognostic variable (vorticity) is integrated in the quasi-geostrophic formalism, whereas primitive equation models typically integrate three prognostic variables (horizontal velocity components, and layer thickness or pressure). Therefore, dynamical compatibility between multiple model variables is one of the main issues tackled in this investigation. Another objective is to benchmark the general performance of this assimilation method, which is based on optimal interpolation and incorporates a number of simplifications in its present implementation, with respect to that of an approximate implementation (ROIF) of Kalman filter.

[41] The Lagrangian assimilation technique is implemented in MICOM, which is a primitive equation, layered ocean model. The reduced-gravity, midlatitude double-gyre ocean model configuration allows for a highly nonlinear interaction between dynamically different ocean flow regimes, while being far simpler than carrying out realistic ocean simulations. The dynamical compatibility between corrected model-velocity and layer-thickness fields is accomplished using a simple and computationally efficient formulation based on geostrophic balance and mass conservation. Lagrangian (OI-Lag) and Pseudo-Lagrangian (OI-PsLag) versions of the assimilation method differ only in the observation operator, in that the Pseudo-Lagrangian operator relates the Lagrangian velocity from drifter data to the Eulerian model velocity, whereas the Lagrangian operator relates the Lagrangian velocity from drifter data to the Lagrangian velocity from model-simulated drifters. Regarding the dynamical compatibility, both Pseudo-Lagrangian and Lagrangian techniques use the same technique. The performance of each technique is compared to that of a Kalman filter method, which is implemented in the Pseudo-Lagrangian mode (KF-PsLag), and provides a general reference for assimilation performance.

[42] On the basis of an extensive set of twin experiments (results from 74 twin experiments are shown here) conducted as a function of two time sampling densities ( $\Delta t = 6$  hours or  $\Delta t = 3$  days) and three space sampling densities (36, 64, and 121 uniformly distributed drifters in  $2000^2$  km<sup>2</sup> ocean basin), the following results are obtained. In the case of  $\Delta t = 6$  hours, where  $\Delta t \ll T_L$  represents an idealistically high time sampling density, all methods (OI-Lag, OI-PsLag, KF-PsLag) offer the same performance, as diagnosed by the relative layer thickness error  $h_{error}(t)$ . In this regime, the performance is a function of only the space sampling density (i.e., the  $e$ -folding timescale of error convergence decreases as space sampling density increases). These results show that both the observation operator and dynamical compatibility relationships of the OI technique work well in the limit of high time sampling. A second set of experiments are carried out for  $\Delta t = 3$  days, which is relevant for oceanographic applications as  $\Delta t \approx T_{Lmin}/2$ . In this case, the Lagrangian observation operator is found to be clearly superior to the Pseudo-Lagrangian observation

operator. For instance, OI-Lag using only 36 drifters yields equivalent performance (and much better for 121 drifters) as for OI-PsLag using 121 drifters. Finally, a third set of experiments is conducted by eliminating the dynamical balancing of the corrected variables. In this case, the response of the ocean model to assimilation is found to slow down drastically, which not only supports the validity of the simple dynamical balancing technique developed here, but also indicates that the correction of model velocity field must be accompanied by an appropriate correction of layer thickness (or pressure, depending on model formulation) for such assimilation to be effective. Finally, a qualitative expression for the MSE of the OI method is derived as a function of time and space sampling densities, and model and observations errors. In the future, more advanced versions of the Lagrangian assimilation scheme (outlined by *Molcard et al.* [2003]) will be considered for implementation in multi-layered OGCMs.

## Appendix A: Derivation of the Error Formula

[43] Let the vector  $\mathbf{z} \equiv \begin{pmatrix} \mathbf{u} \\ \mathbf{v} \end{pmatrix}$  be a vector characterizing the ocean state over a given region at a given time for a specific circulation model, where  $\mathbf{u}$  and  $\mathbf{h}$ , respectively, denote the components directly observable and unobservable from the measurements. For this paper, we can interpret  $\mathbf{u}$  as the Eulerian vector field on a given grid during given run time  $T_{ob}$  and  $\mathbf{h}$  as corresponding set of the layer thickness fields. Let  $\mathbf{y}$  be the observed position increments computed from a set of particle trajectories observed during the same time period  $T_{ob}$ . Then, Bayesian probabilistic arguments under a Gaussian distribution [e.g., *Lorenc*, 1986] leads to the following, well-documented formula to combine the model output with observation:

$$\mathbf{z}^a = \mathbf{z}^b + \Delta\mathbf{z}, \quad \Delta\mathbf{z} = \mathbf{A}(\mathbf{y} - \mathbf{H}(\mathbf{z}^b)), \quad (\text{A1})$$

where

$$\mathbf{A} = \mathbf{R}^b \mathbf{G}^T (\mathbf{G} \mathbf{R}^b \mathbf{G}^T + \mathbf{R}^o)^{-1}, \quad (\text{A2})$$

$\mathbf{z}^a$  is the model state vector after assimilation,  $\mathbf{z}^b$  is the model state vector before assimilation,  $\mathbf{y}$  is the vector of observations,  $\mathbf{H}(\mathbf{z}^b)$  is the functional that relates model state variables to the observations,  $\mathbf{R}^o$  is the observation error covariance matrix,  $\mathbf{R}^b$  is the covariance matrix of the model uncertainty, superscript  $T$  stands for transposition, and, finally

$$\mathbf{G} = \frac{\delta \mathbf{H}(\mathbf{z}^b)}{\delta \mathbf{z}^b}$$

is the derivative of the model-to-observation functional (sensitivity matrix).

[44] If  $\mathbf{h}$  and  $\mathbf{u}$  are related linearly and deterministically as  $\mathbf{h} = \mathbf{L}\mathbf{u}$  where  $\mathbf{L}$  is a matrix of appropriate dimensions, then by linearity  $\Delta\mathbf{h} = \mathbf{L}\Delta\mathbf{u}$  (which can also be shown to be formally consistent with A1 and A2). In our specific context,  $\mathbf{L}$  is the operator combining the inversion of equation (4) and mass-balance formula (5). By virtue of the deterministic relation, the Bayesian estimation (equa-

tions (A1) and (A2)) can be carried out only for  $\mathbf{u}$  (i.e.,  $\mathbf{z}$  without  $\mathbf{h}$ ), substantially reducing the matrix dimensions and hence computational cost.

[45] If the functional  $\mathbf{H}(\mathbf{z})$  is linear, then  $\mathbf{G}$  is constant and in this case the matrix mean square error (MSE) of equations (A1) and (A2) is given by

$$\mathbf{S} \equiv \langle (\mathbf{z}^a - \mathbf{z})(\mathbf{z}^a - \mathbf{z})^T \rangle = \mathbf{R}^b - \mathbf{A}\mathbf{G}\mathbf{R}^b. \quad (\text{A3})$$

Also, MSEs for the components  $\mathbf{u}$  and  $\mathbf{h}$  satisfy

$$\mathbf{S}_h \equiv \mathbf{L}\mathbf{S}_u\mathbf{L}^T.$$

If matrix  $\mathbf{S}_u$  is diagonal  $\mathbf{S}_u = \mathbf{s}_u^2\mathbf{I}$ , i.e., covariances of assimilation errors for velocity are negligible,  $\mathbf{L}$  is orthogonal, then the relative error in estimating  $\mathbf{h}$ ,

$$\delta_h \equiv \sqrt{\frac{Sp(S_h)}{\mathbf{h}^T\mathbf{h}}} = \frac{s_u}{\|\mathbf{u}\|} \equiv \delta_u,$$

coincides with the relative error of the velocity ( $Sp$  stands for the trace of matrix). If  $\mathbf{L}$  is not orthogonal, but instead is an integral (smoothing) operator, then it can be shown that

$$\delta_h \leq \delta_u. \quad (\text{A4})$$

[46] On the other hand, if  $\mathbf{H}(\mathbf{z})$  is nonlinear, the error formulas above are less meaningful. For this reason, we give an error estimate for the specific assimilation procedure (equations (6), (7), and (8)). Let  $\mathbf{u}_{ij}(n)$  be the true velocity. From equations (7) and (8),

$$\begin{aligned} s_{ij}^2 &= \mathcal{E} \left\{ \left( \mathbf{u}_{ij}^a(n) - \mathbf{u}_{ij}(n) \right)^2 \right\} \\ &= \sigma_b^2 + 2\beta \sum_{m=1}^M \mathcal{E} \left\{ \chi_{ij}(\mathbf{r}_m(n)) (\mathbf{v}_m^o(n) - \mathbf{v}_m^b(n)) \right. \\ &\quad \cdot \left. \left( \mathbf{u}_{ij}^b(n) - \mathbf{u}_{ij}(n) \right) \right\} + \beta^2 \sum_{m_1=1}^M \sum_{m_2=1}^M \mathcal{E} \left\{ \chi_{ij}(\mathbf{r}_{m_1}(n)) \chi_{ij} \right. \\ &\quad \cdot \left. \left( \mathbf{r}_{m_2}(n) \right) \left( \mathbf{v}_{m_1}^o(n) - \mathbf{v}_{m_1}^b(n) \right) \cdot \left( \mathbf{v}_{m_2}^o(n) - \mathbf{v}_{m_2}^b(n) \right) \right\}, \quad (\text{A5}) \end{aligned}$$

where  $\mathcal{E}\{\}$  is the operator of averaging over the ensemble and relation

$$\mathcal{E} \left\{ \left( \mathbf{u}_{ij}^b(n) - \mathbf{u}_{ij}(n) \right)^2 \right\} = \sigma_b^2$$

was used. To simplify the sums, notice that for any two random variables  $\xi$  and  $\eta$ ,

$$\mathcal{E}\{\chi_A(\xi)\eta\} = \mathcal{P}(\xi \in A)\mathcal{E}\{\eta|\xi \in A\},$$

where  $\chi_A(\xi)$  is the indicator of the set  $A$ . Further, we apply that to the case where  $A$  is a fixed mesh and  $\xi$  is the drifter position. If the drifter is inside of the mesh, we can use the following decomposition:

$$\mathbf{v}_m^b(n) \approx \mathbf{u}_{ij}^b(n) - \frac{1}{2}\mathbf{D}_{ij}^b(n)\mathbf{u}_{ij}^b(n),$$

where  $\mathbf{D}_{ij}^b(n)$  is defined in equation (11). Assuming local homogeneity of the deviation  $\mathbf{u}^b(t, \mathbf{r}) - \mathbf{u}(t, \mathbf{r})$  we conclude that  $\mathbf{D}_{ij}^b(n)$  is independent of  $\mathbf{u}_{ij}^b(n)$ . This assumption allows

us to split the correlations for the velocity field and its gradient. Then, taking into account that the observations and model are statistically independent, we get for the conditional expectations, given the particles are inside the mesh,

$$\begin{aligned} \mathcal{E} \left\{ \left( \mathbf{v}_{m_1}^o - \mathbf{v}_{m_1}^b \right) \cdot \left( \mathbf{v}_{m_2}^o - \mathbf{v}_{m_2}^b \right) \middle| \mathbf{r}_{m_1} \in \mathbf{S}_{ij}, \mathbf{r}_{m_2} \in \mathbf{S}_{ij} \right\} &\approx \sigma_b^2(1 + \varepsilon^2) \\ &+ \sigma_o^2 \mathcal{E} \left\{ \left( \mathbf{v}_m^o - \mathbf{v}_m^b \right) \cdot \left( \mathbf{u}_{ij}^b - \mathbf{u}_{ij} \right) \middle| \mathbf{r}_m(n) \in \mathbf{S}_{ij} \right\} \approx -\sigma_b^2, \end{aligned}$$

where  $\varepsilon$  is defined in equation (14). We omitted argument  $n$  assuming a fixed moment. Thus, for the unconditional expectations,

$$\mathcal{E} \left\{ \left( \mathbf{v}_{m_1}^o - \mathbf{v}_{m_1}^b \right) \cdot \left( \mathbf{v}_{m_2}^o - \mathbf{v}_{m_2}^b \right) \right\} \approx p_{m_1 m_2} (\sigma_b^2(1 + \varepsilon^2) + \sigma_o^2)$$

$$\mathcal{E} \left\{ \left( \mathbf{v}_m^o - \mathbf{v}_m^b \right) \cdot \left( \mathbf{u}_{ij}^b - \mathbf{u}_{ij} \right) \right\} \approx -\sigma_b^2 p_m,$$

where

$$p_m = P(\mathbf{r}_m \in \mathbf{S}_{ij}), \quad \mathbf{p}_{m_1 m_2} = \mathbf{P}(\mathbf{r}_{m_1} \in \mathbf{S}_{ij}, \mathbf{r}_{m_2} \in \mathbf{S}_{ij}).$$

Let  $\nu_{ij}$  be the number of drifters in the mesh at the given moment and  $\mu_{ij}^{(1)} = \langle \nu_{ij} \rangle$ ,  $\mu_{ij}^{(2)} = \langle \nu_{ij}^2 \rangle$  its mean and the second moment. Notice that

$$\sum_m p_m = \mu_{ij}^{(1)}, \quad \sum_{m_1 m_2} p_{m_1 m_2} = \mu_{ij}^{(2)}.$$

Then, after substituting all the above into equation (A5) we get the following:

$$s_{ij}^2 = \sigma_b^2 \left( 1 - 2\mu_{ij}^{(1)}\beta + \mu_{ij}^{(2)}\beta^2(1 + \varepsilon^2) \right) + \mu_{ij}^{(2)}\beta^2\sigma_o^2. \quad (\text{A6})$$

As the result, the relative MSE is given by

$$\delta_{ij}^2 = \gamma \left( 1 - 2\mu_{ij}^{(1)}\beta + \mu_{ij}^{(2)}\beta(1 + \beta\varepsilon^2) \right).$$

There can be different assumptions for drifter locations allowing to specify  $\mu_{ij}^{(1)}$  and  $\mu_{ij}^{(2)}$ . For example, if there is exactly one particle in the considered mesh at given moment, then  $\mu_{ij}^{(1)} = \mu_{ij}^{(2)} = 1$  and

$$\delta_{ij}^2 = \gamma(1 - \beta + \beta^2\varepsilon^2).$$

If one sets  $\varepsilon = 0$ , then the latter turns to the well-known MSE (equation (A3)) obtained from the linear theory

$$\delta_{ij}^2 = \gamma(1 - \beta) = \gamma\sigma_o^2 / (\sigma_b^2 + \sigma_o^2).$$

Now consider the relative MSE averaging through the basin,

$$\delta_u^2 = \frac{\sum_{ij} s_{ij}^2}{\sum_{ij} u_{ij}^2}.$$

Assuming homogeneity of the velocity through the basin we get from equation (A6)

$$\delta_u^2 = \gamma(1 - 2\mu_1\beta + \mu_2\beta(1 + \beta\varepsilon^2)),$$

where

$$\mu_1 = \frac{1}{K} \sum_{ij} \langle v_{ij} \rangle = \frac{M}{K}, \quad \mu_2 = \frac{1}{K} \sum_{ij} \langle v_{ij}^2 \rangle,$$

$K$  is the total number of grid-points and  $M$  is the number of particles. Again, if there is exactly one particle in each grid, then

$$\mu_2 \equiv \mu_1 \equiv \mu = M/K,$$

and we arrive at equation (12) while equation (13) follows directly from equation (A4).

[47] **Acknowledgments.** The authors greatly appreciate the support of the Office of Naval Research under grants N00014-97-1-0620 and N00014-99-1-0049 (A. Molcard, A. Griffa, and T. M. Özgökmen), N00014-99-1-0042 (L. I. Piterberg), N00014-95-1-0257 and N00014-99-1-1066 (T. M. Chin). The authors have greatly benefited from discussions with M. Iskandarani, N. Pinardi and A. Mariano.

## References

- Bauer, S., M. S. Swenson, A. Griffa, A. J. Mariano, and K. Owens, Eddy-mean flow decomposition and eddy-diffusivity estimates in the tropical Pacific Ocean, *J. Geophys. Res.*, *103*, 30,855–30,871, 1998.
- Bleck, R., and E. P. Chassignet, Simulating the oceanic circulation with isopycnic-coordinate models, in *The Oceans: Physical-Chemical Dynamics and Human Impact*, edited by S. K. Majumbar and W. E. Miller, pp. 17–39, Pa. Acad. of Sci., Easton, Pa., 1994.
- Bleck, R., C. Rooth, D. Hu, and L. T. Smith, Ventilation and mode water formation in a wind- and thermohaline-driven isopycnic coordinate model of the North Atlantic, *J. Phys. Oceanogr.*, *22*, 1486–1505, 1992.
- Castellari, S., A. Griffa, T. M. Özgökmen, and P.-M. Poulain, Prediction of particle trajectories in the Adriatic Sea using Lagrangian data assimilation, *J. Mar. Syst.*, *29*, 33–50, 2001.
- Chin, T. M., A. J. Mariano, and E. P. Chassignet, Spatial regression with Markov random fields for Kalman filter approximation in least-squares solution of oceanic data assimilation problems, *J. Geophys. Res.*, *104*, 1233–1257, 1999.
- Chin, T. M., A. C. Haza, and A. J. Mariano, A reduced-order information filter for multi-layer shallow water models: Profiling and assimilation of sea surface height, *J. Atmos. Oceanic Technol.*, *19*(4), 517–533, 2002.
- Coulliette, C., and S. Wiggins, Intergyre transport in a wind-driven, quasi-geostrophic double gyre: An application of lobe dynamics, *Nonlinear Processes Geophys.*, *7*, 59–85, 2000.
- Davis, R. E., Observing the general circulation with floats, *Deep Sea Res.*, *38*, 5531–5571, 1991.
- Falco, P., A. Griffa, P.-M. Poulain, and E. Zambianchi, Transport properties in the Adriatic Sea deduced from drifter data, *J. Phys. Oceanogr.*, *30*, 2055–2071, 2000.
- Fratantoni, D. M., North Atlantic surface circulation during the 1990's observed with satellite-tracked drifters, *J. Geophys. Res. Oceans*, *106*, 22,067–22,093, 2001.
- Garraffo, Z. D., A. J. Mariano, A. Griffa, C. Veneziani, and E. P. Chassignet, Lagrangian data in a high-resolution numerical simulation of the North Atlantic: 1. Comparison with in situ drifter data, *J. Mar. Syst.*, *29*, 157–176, 2001.
- Ghil, M., and P. Malanotte-Rizzoli, Data assimilation in meteorology and oceanography, *Adv. Geophys.*, *33*, 141–266, 1991.
- Griffa, A., Applications of stochastic particle models to oceanographic problems, in *Stochastic Modelling in Physical Oceanography*, edited by R. Adler, P. Muller, and B. Rozovskii, pp. 113–128, Birkhauser, Boston, 1996.
- Griffa, A., K. Owens, L. Piterberg, and B. Rozovskii, Estimates of turbulence parameters from Lagrangian data using a stochastic particle model, *J. Mar. Res.*, *53*, 212–234, 1995.
- Hansen, D. V., and P.-M. Poulain, Quality control and interpolations of WOCE/TOGA drifter data, *J. Atmos. Oceanic Technol.*, *13*, 900–909, 1996.
- Hernandez, F., P. Y. Le Traon, and N. H. Barth, Optimizing a drifter cast strategy with a genetic algorithm, *J. Atmos. Oceanic Technol.*, *12*, 330–345, 1995.
- Holland, W. R., The role of mesoscale eddies in the general circulation of the ocean, *J. Phys. Oceanogr.*, *22*, 1033–1046, 1978.
- Ishikawa, Y. I., T. Awaji, and K. Akimoto, Successive correction of the mean sea surface height by the simultaneous assimilation of drifting buoy and altimetric data, *J. Phys. Oceanogr.*, *26*, 2381–2397, 1996.
- Kamachi, M., and J. J. O'Brien, Continuous assimilation of drifting buoy trajectory into an equatorial Pacific ocean model, *J. Mar. Syst.*, *6*, 159–178, 1995.
- Kuznetsov, L., M. Toner, A. D. Kirwan, C. K. R. T. Jones, L. H. Kantha, and J. Choi, The Loop Current and adjacent rings delineated by Lagrangian analysis of near-surface flow, *J. Mar. Res.*, *60*, 405–429, 2002.
- Lavender, K. L., R. E. Davis, and W. B. Owens, Direct velocity measurements in the Labrador and Irminger Seas describe pathways of Labrador Sea Water, *Nature*, *407*, 66–69, 2000.
- Lorenc, A. C., Analysis methods for numerical weather prediction, *Q. J. R. Meteorol. Soc.*, *112*, 1177–1194, 1986.
- Mariano, A. J., A. Griffa, T. M. Özgökmen, and E. Zambianchi, Lagrangian analysis and predictability of coastal and ocean dynamics 2000, *J. Atmos. Oceanic Technol.*, *19*, 1114–1126, 2002.
- McClellan, J. L., P.-M. Poulain, and J. W. Pelton, Eulerian and Lagrangian statistics from surface drifters and a high-resolution POP simulation in the North Atlantic, *J. Phys. Oceanogr.*, *32*, 2472–2491, 2002.
- Mead, J. L., and A. F. Bennett, Towards regional assimilation of Lagrangian form of the shallow water model and its inverse, *J. Mar. Syst.*, *29*, 365–384, 2001.
- Molcard, A., L. I. Piterberg, A. Griffa, T. M. Özgökmen, and A. J. Mariano, Assimilation of drifter observations for the reconstruction of the Eulerian circulation field, *J. Geophys. Res.*, *108*, 3056, doi:10.1029/2001JC001240, 2003.
- Owens, W. B., A statistical description of the mean circulation and eddy variability in the northwestern Atlantic using SOFAR floats, *Prog. Oceanogr.*, *28*, 257–303, 1991.
- Özgökmen, T. M., A. Griffa, L. I. Piterberg, and A. J. Mariano, On the predictability of the Lagrangian trajectories in the ocean, *J. Atmos. Oceanic Technol.*, *17*, 366–383, 2000.
- Özgökmen, T. M., L. I. Piterberg, A. J. Mariano, and E. H. Ryan, Predictability of drifter trajectories in the tropical Pacific Ocean, *J. Phys. Oceanogr.*, *31*, 2691–2720, 2001.
- Piterberg, L. I., Short term prediction of Lagrangian trajectories, *J. Atmos. Oceanic Technol.*, *18*, 1398–1410, 2001a.
- Piterberg, L. I., The top Lyapunov exponent for a stochastic flow modeling the upper ocean turbulence, *SIAM J. Appl. Math.*, *62*, 777–800, 2001b.
- Piterberg, L. I., and T. M. Özgökmen, A simple prediction algorithm for the Lagrangian motion in two-dimensional turbulent flows, *SIAM J. Appl. Math.*, *63*, 116–148, 2002.
- Poje, A. C., and G. Haller, Geometry of cross-stream mixing in a double-gyre ocean model, *J. Phys. Oceanogr.*, *29*, 1649–1665, 1999.
- Poje, A. C., M. Toner, A. D. Kirwan Jr., and C. K. R. T. Jones, Drifter launch strategies based on Lagrangian templates, *J. Phys. Oceanogr.*, *32*, 1855–1869, 2002.
- Poulain, P.-M., Adriatic Sea surface circulation as derived from drifter data between 1990 and 1999, *J. Mar. Syst.*, *29*, 3–32, 2001.
- Smith, R. D., M. E. Maltrud, F. O. Bryan, and M. W. Hecht, Numerical simulation of the North Atlantic Ocean at 1/10°, *J. Phys. Oceanogr.*, *30*, 1532–1561, 2000.
- Swenson, M. S., and P. P. Niiler, Statistical analysis of the surface circulation of the California Current, *J. Geophys. Res.*, *101*, 22,631–22,645, 1996.
- Thomson, D. J., A random walk model of dispersion in turbulent flows and its application to dispersion in a valley, *Q. J. R. Meteorol. Soc.*, *112*, 511–529, 1986.
- Toner, M., A. C. Poje, A. D. Kirwan, C. K. R. T. Jones, B. L. Lipphardt, and C. E. Grosch, Reconstructing basin-scale Eulerian velocity fields from simulated drifter data, *J. Phys. Oceanogr.*, *31*, 1361–1376, 2001a.
- Toner, M., A. D. Kirwan, L. H. Kantha, and J. K. Choi, Can general circulation models be assessed and their output enhanced with drifter data?, *J. Geophys. Res.*, *106*, 19,563–19,579, 2001b.
- Wiggins, S., *Chaotic Transport in Dynamical Systems*, 301 pp., Springer-Verlag, New York, 1992.
- Zhang, H. M., M. D. Prater, and T. Rossby, Isopycnal Lagrangian statistics from the North Atlantic Current RAFOS float observations, *J. Geophys. Res.*, *106*, 13,817–13,836, 2001.

T. M. Chin, A. Griffa, A. Molcard, and T. M. Özgökmen, Meteorology and Physical Oceanography, Rosenstiel School of Marine and Atmospheric Sciences, University of Miami, 4600 Rickenbacker Causeway, Miami, FL 33149-1098, USA. (tmchin@rsmas.miami.edu; agriffa@rsmas.miami.edu; amolcard@rsmas.miami.edu; tozokmen@rsmas.miami.edu)

L. I. Piterberg, Center for Applied Mathematical Sciences, University of Southern California, 1042 West 36th Place, DRB-330, Los Angeles, CA 90089-1113, USA. (piter@math.usc.edu)